Scripta Materialia 194 (2021) 113706

Contents lists available at ScienceDirect

Scripta Materialia

journal homepage: www.elsevier.com/locate/scriptamat

Hybrid diffusive-displacive helium outgassing in Cu/Nb multilayer composites

Rui Gao[a], Miaomiao Jin[b,*], Qing-Jie Li[a], Kang Pyo So[a], Lifeng Zhang[c,d], Xianping Wang[c], Qianfeng Fang[c], Cheng Sun[e], Lin Shao[f], Ju Li[a,g,*]

[a] Department of Nuclear Science and Engineering, Massachusetts Institute of Technology, Cambridge, MA 02139, USA
[b] Department of Nuclear Engineering, The Pennsylvania State University, University Park, 205 Hallowell Building, PA 16802, USA
[c] Key Laboratory of Materials Physics, Institute of Solid State Physics, Chinese Academy of Sciences, Hefei, 230031, PR China
[d] Department of Materials Science and Engineering, University of Science and Technology of China, Hefei, 230026, PR China
[e] Characterization and Advanced PIE Division, Idaho National Laboratory, Idaho Falls, ID 83415, USA
[f] Department of Nuclear Engineering, Texas A&M University, College Station, TX 77845, USA
[g] Department of Materials Science and Engineering, Massachusetts Institute of Technology, Cambridge, MA 02139, USA

ARTICLE INFO

Article history:
Received 16 September 2020
Revised 26 December 2020
Accepted 28 December 2020
Available online 12 January 2021

Keywords:
Thermal desorption spectroscopy
In-situ TEM heating
Helium bubble coalescence
Fracture
Surface blister

ABSTRACT

Gas generation degrades material properties in nuclear applications. The construction of self-assembled bubble channels was proposed to help release gas to the surface. In this study, thermal desorption spectroscopy, in-situ TEM heating and molecular dynamics simulations were carried out to assess the outgassing feasibility in helium-irradiated Cu/Nb multilayers with low structural damage. We found that the formation of outgassing networks has a hybrid diffusive-displacive nature, with diffusive bubble coalescence and crack-induced displacive fracture. The latter could destroy the integrity of the multilayer structure. This suggests that the outgassing strategy making use of self-assembled cavity networks should be carefully designed to avoid large-scale structural failure.

Helium as a transmutation product in nuclear reactors triggers serious degradation of structural materials. Significant efforts have been made to reduce helium damages by increasing the density of nanoscaled defect sinks, since otherwise when the segregation of helium to a 2D grain boundary (GB) network (say with 5μm grain size [1]) reaches monolayer coverage throughout the GB network, a spatially percolating intergranular crack system is created, which would be the most damaging to a metal's integrity. Instead of trapping helium, another strategy could be to outgas/vent helium to the surface. This outgassing process could be achieved via the construction of "vascular" channels [3,4]. While both helium-filled 1D channels and 2D crevices can vent and reduce the helium inventory (thermodynamically, helium has purely repulsive interactions with the metal and does not want to stay in the metal), based on linear elasticity and fracture mechanics, a percolating 1D channel system would be much less damaging to a metal's mechanical integrity than a percolating 2D crack system, due to non-singular stress amplification factor (prolate/cylindrical voids are much better than oblate voids) from fracture mechanics viewpoint.

Generally speaking, for the stated outgassing strategy to work, we would like the outgassing process to be continuous and gentle, not abrupt and destructive. A traditional theory for outgassing by Evans [2], however, described a violent fracture process where the helium pressure is high enough to cause a sudden vertical displacement that blows out a surface blister lid. Evans modeled the dependence of the blister lid thickness ("Deckeldicke") as a function of the material fracture strength. In this scenario, the gas release comes at a great cost to the mechanical integrity of the material, because the process is entirely displacive (specifically, tensile opening displacement), and Evans envisioned an "essentially athermal", diffusionless process. We naturally wonder if there can be some diffusional reconstructions, whereby the outgassing can be more gentle and continuous in time, e.g. with surface-diffusion enabled bubble coalescence, that are perhaps templated by 1D nanodispersions like carbon nanotubes that could form a 1D percolating vascular network [3], or by 2D nano-phase boundaries with special crystallographic characters that could promote the bubble coalescence during helium irradiation [4,5]. In any case, one wonders if a templated diffusive self-organization of the helium-filled cavities, with gradual but systematic outgassing networks connecting to the free surfaces, could be the key to gentle, continuous helium discharge, with minimal structural damage.

* Corresponding authors.
E-mail addresses: mmjin@psu.edu (M. Jin), liju@mit.edu (J. Li).

https://doi.org/10.1016/j.scriptamat.2020.113706
1359-6462/

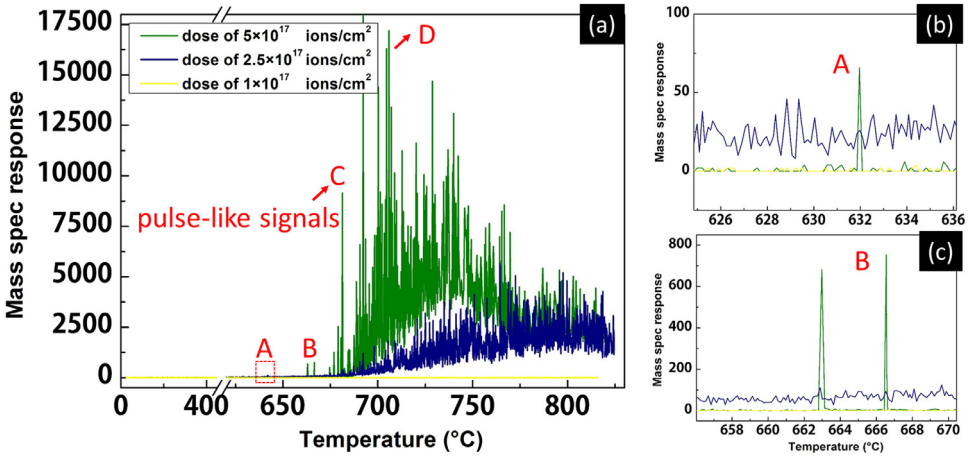

Fig. 1. (a) Thermal desorption spectra of helium-charged Cu/Nb bulk composites with different implantation fluences during the heating. (b) and (c) The helium signals appearing at lower temperatures in the image (a) are enlarged.

In this work, we examine a particular Cu/Nb layered nanocomposite [6] and explore its templating effect on the self-organized outgassing, by careful structural characterization and quantitative measurement of helium outgassing kinetics after accelerator-based helium-irradiation. The evolution of helium bubbles is revealed by in-situ TEM heating experiments and atomistic simulations. Unfortunately, while there are definitely extensive, hierarchical diffusive self-organizations at the nanoscale, at the macro scale the outgassing kinetics is still dominated by violent bursts that are controlled by displacive fractures. These results suggest that the outgassing strategy needs to be carefully designed to avoid large-scale structural failure.

We fabricated Cu/Nb nanolaminate by the accumulative roll bonding (ARB) technique, as detailed in ref. [7]. Bulk Cu/Nb laminates were first irradiated by 300 keV He ions with different fluences at room temperature (RT). We then performed thermal desorption spectroscopy (TDS) analysis on these irradiated samples to detect helium gas release. Specifically, TDS was measured using a quadrupole mass spectrometer (QMS) under a vacuum of ~10^{-9} Torr and the temperature was raised from RT to 820°C. The in-situ heating experiment was carried out in a JEOL 2010F transmission electron microscope (TEM) to examine helium bubble evolution and helium outgassing mechanisms. The TEM cross-sectional lamella was prepared by focused ion beam (FIB) at 30 kV followed by low energy cleaning at 2 kV. Helium concentration and radiation damage as a function of depth were estimated by the SRIM (Stopping and Range of Ions in Solids) software [8]. We used 29 eV and 41 eV as the average threshold displacement energies for Cu and Nb, respectively, in the SRIM calculation.

Molecular dynamics (MD) simulations using the LAMMPS package [9] were performed to simulate helium bubble evolution during heating. The interatomic interactions are described by an EAM potential by Kashinath and Demkowicz [10]. The simulation box was constructed by two halves of FCC Cu and BCC Nb, containing a total of 572,596 atoms. To mimic the post-irradiation bubbles, a random distribution of bubbles with a helium/vacancy ratio of 2.0 was created over the Cu and Nb bulks, and the interface (see a series of schematic demonstration in Supporting Information). The system was first adequately relaxed at 400 K for 100 ps, under zero pressure. Then temperature was ramped up from 400 K to 1200 K over 10 ns using the isothermal–isobaric setting.

We first examined the outgassing capacity of helium-irradiated bulk multilayer samples by tracking helium release during TDS experiments. Fig. 1a shows the mass spectrometry (i.e., the relative amount of released gas) for samples irradiated at three different helium implantation doses, 10^{17}, 2.5 × 10^{17} and 5 × 10^{17} ions/cm^2, respectively, at a heating rate of 10°C/min. For convenience, we denote the three samples as the low-dose sample, medium-dose sample and high-dose sample, respectively. For the high-dose sample (green line in Fig. 1a), macroscopic helium release is detected starting at 632°C (red dashed box in Fig. 1a, enlarged in Fig. 1b). As temperature increases, the rate of gas release starts to increase. For example, the peak heights in the range of 663 - 667°C (labeled as peak *B* in Fig. 1a, enlarged in Fig. 1c) are almost one order of magnitude higher than that at 632°C. Massive bursting releases featured by many overlapping pulse-like signals appear at around 700°C, after which helium release slows down. In the medium-dose sample (blue line in Fig. 1a), weak helium signals appear before the first peak in the high-dose sample (Fig. 1b); however, the massive release is delayed to higher temperatures and the overall spectrum becomes wider. For the low-dose sample, no helium escape is detected in the entire temperature range from 400 to 825°C. It was previously reported that helium atoms can be thermally desorbed from monovacancy or divacancy at about 400°C from within helium (a few keV) irradiated single-crystal copper [11], signifying diffusive activities can commence at 400°C in pure Cu (melting point of 1356.6 K). In that study, with a few keV kinetic energy, the helium penetration depth is tens of nanometers from the incident surface, while in our case with 300 keV implantation, the depth is about 800 nm. Hence, the desorption temperature is much higher due to increased helium depth and difficult helium diffusion perpendicular to Cu/Nb interfaces (Nb's melting point is 2742 K). Moreover, given the macroscopic size of the sample (5 mm in length by 5 mm in width), the amount of desorbed helium reaching side surfaces at around 400°C would be low enough to be beyond detection by macroscopic TDS.

Next, we performed an in-situ heating experiment of a microscopic specimen of 150 nm thickness inside the TEM to observe the evolution of helium bubbles that mechanistically should be relevant to helium outgassing. To this end, a helium-irradiated Cu/Nb lamella was in-situ heated to 500°C with a rate of 30°C/min in TEM. The initial helium bubble morphologies are shown in Supporting Information Fig. S1. We found that bubbles in the Nb layers only show negligible changes in both bubble size and number density during the heating process. Therefore, in the following, we mainly focus on bubble dynamics in the Cu layers. In the initial heating period from 100°C to 300°C, individual bubbles located at interfaces (Fig. 2a) gradually coarsen and wet interfaces, as depicted by continuous bright "lines" in Fig. 2b. Then heating from 300°C to 430°C results in quite dramatic diffusive bubble re-

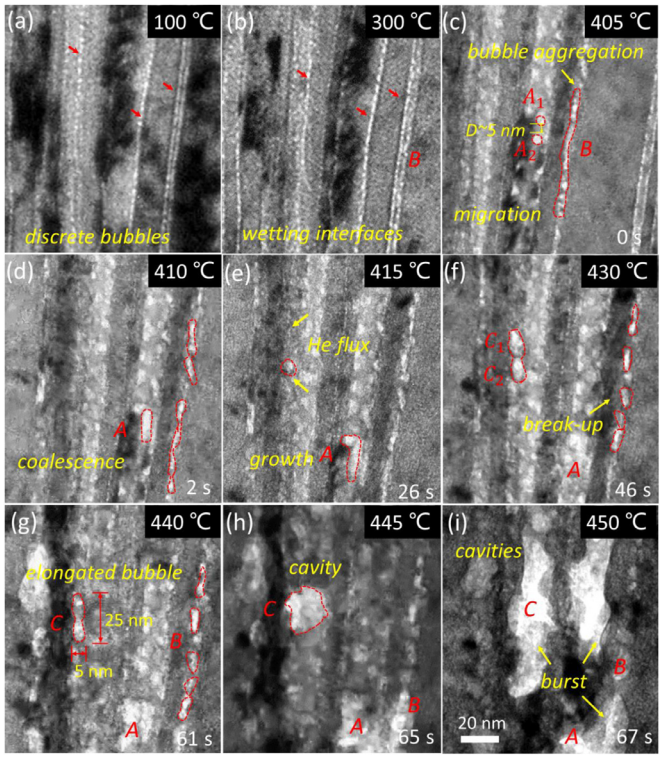

Fig. 2. Dynamical characteristics of helium bubbles. Snapshots are extracted from video S1 during the in-situ heating experiment. (a and b) Discrete bubbles wet interfaces and coarsen during the heating from RT to 300°C. (c and d) Bubbles A_1 and A_2 migrate and merge into an elongated bubble within 2 seconds. (b–f) Tiny bubbles confined in an ultra-thin Cu layer (region B) coalesce into a highly elongated bubble aggregation which then broke up into short chains as temperature increases. (e–g) Bubbles C_1 and C_2 slowly expand and coalesce within about 35 seconds through the helium diffusion. (h–i) Bubble reorganizations suddenly blow-up and transform into cavities at the nanoscale. (See video S1 for the entire evolution process).

organizations such as migration and coalescence, surface blunting, and Plateau–Rayleigh instability. See video S1 (8 × accelerated) in Supporting Information and typical snapshots (Fig. 2c–g) for details. Fig. 2c and d demonstrates the bubble coalescence process. When the temperature exceeds 400°C, two small bubbles (A_1 and A_2) initially separated by 5 nm migrate towards each other within two seconds and merge into an elongated bubble with a length of 20 nm (Fig. 2d and e). Meanwhile, bubbles in region B (Fig. 2c) spontaneously coalesce within a couple of minutes. Although this bubble agglomeration (tens of nanometers in length) is confined in an ultra-thin Cu layer (thickness of about 6~7 nm), it subsequently breaks up into discrete elongated bubbles (Fig. 2c–f) at around 430°C due to the Plateau-Rayleigh (P-R) instability [12]. The high-temperature enhanced diffusion of small helium clusters also contributes to bubble expansion, as shown by C1 and C2 in Fig. 2e and f. Those bubbles then slowly coarsen and coalesce into an elongated bubble (see Fig. 2e–g within ~35 s). As the temperature reaches ~450°C, elongated bubbles such as C in Fig. 2g (with around 20~30 nanometers in length from a cross-sectional view) abruptly burst (Fig. 2h and i and video S1). This transition from more gentle diffusive-dominated bubble coalescence to abrupt displacive-dominated fracture is attributed to the cavity size growing to a critical flaw size from fracture mechanics: $(\sigma_\infty + P_{He})\sqrt{\pi a} < K_{IC}$, where K_{IC} is the critical stress intensity factor, a is the radius of an oblate cavity, σ_∞ is far-field tensile stress, and P_{He} is the internal helium pressure which increases with temperature.

We further carried out MD simulations to unveil the details of bubble coalescence during heating with a given pre-existing bubble distribution. Note that MD simulations are very limited in timescale, hence, to observe bubble motion in a reasonable time frame, the heating temperature is artificially enhanced. However, provided the "clock speed" of evolutions is from a single kinetic parameter, surface diffusivity, which is uniformly accelerated, the observed phenomena can still reflect the current experimental results. Fig. 3 demonstrates the bubble morphology at the interface, Cu bulk, and Nb bulk at selected timestamps (see dynamic evolution in Supporting Information video S2). In the planar view of the MD simulation box (Fig. 3a–c and video S3), tiny bubbles prefer to coalesce at the Cu/Nb interface through bubble coarsening and migration. To minimize strain energy, such self-organization leads to an oblate or a "pancake" cavity morphology [13] at the interface. Also, the majority of bubbles in the Nb layer remain much smaller than those in the Cu layer (Fig. 3d–f and Video S4), in good accordance with the experimental observations. Bubble migration (pointed by black arrows) was occasionally observed in Nb for small size bubbles. As illustrated in Fig. 3g–i (and video S5), due to smaller bubble spacing in the dotted box, a high density of bubbles in Cu can promote the larger-scale coalescence if given a longer time. These "pancake"-like diffusive agglomerations are not yet cracks, since we identify a "crack" by two basic characteristics: (a) an aspect ratio of >10 between the major axes and minor axis of an oblate-shaped flaw, (b) a propensity for opening displacement upon internal or external loading. Because of the limited timescale of MD simulations, we have not yet reached the aspect ratio (a), nor the flaw size (b) required for the transition from diffusive to the abrupt displacive regime of growth in the simulation, and have only seen diffusive coalescence. Obviously, in reality, for the purpose of gentle outgassing, one needs to strike a delicate balance between flaw connectivity/percolation distance and cracking tendency, thus there is a theoretical preference for 1D networks [3,4]. But this may not be achievable in the present material system, due to a strong tendency toward forming outgassing networks that consist of oblate pancakes, crevices and cracks.

According to the macroscopic TDS measurement, no helium release occurs at around 450°C despite the formation of bubble self-organizations in copper at the nanoscale, therefore, it is critical to explore how helium-filled-cavities evolve at the subsequent higher temperatures. We used FIB to cut cross-sectional TEM lamellae from smooth (Fig. 4a) and relatively flat blistering surfaces (with small convexity, as shown in the red dashed box in Fig. 4b) in the low-dose and high-dose samples after TDS measurements, respectively. Fig. 4c shows that the low-dose sample retains an intact layered structure below the blister-free surface (the dashed box in Fig. 4a). Specifically, as shown in the TEM image of Fig. 4e, no nano- or micron-sized cracks are observed in the layered structure, except for many coarsening bubbles and elongated bubbles (tens of nanometers in length) in the helium peak region (~4 at.%). In contrast, the high-dose sample (Fig. 4d) develops long cavities in the helium peak region (see more details in Fig. S2). The enlarged image (Fig. 4f) of the dashed box in Fig. 4d shows the layer morphology in two regions (I and II), with low (<5 at.%) and high (5~15 at.%) helium concentrations, respectively. In region I (Fig. 4g), bubble self-organizations with diameters of 2~5 nm are confined within Cu layers. In region II (Fig. 4f) with a high helium concentration, long cavities are observed, and some previously faceted and equiaxed bubbles (see Fig. S1c, within a 20 nm-thick layer) transformed into quasi-spherical shape during the heating process via surface energy minimization. Moreover, different from the intact blistering surface, Fig. 4i shows that cracks appear on the large blister lids (such as the blister with a diameter of ~ 20 μm in the white dashed box in Fig. 4b), which can extend below the inci-

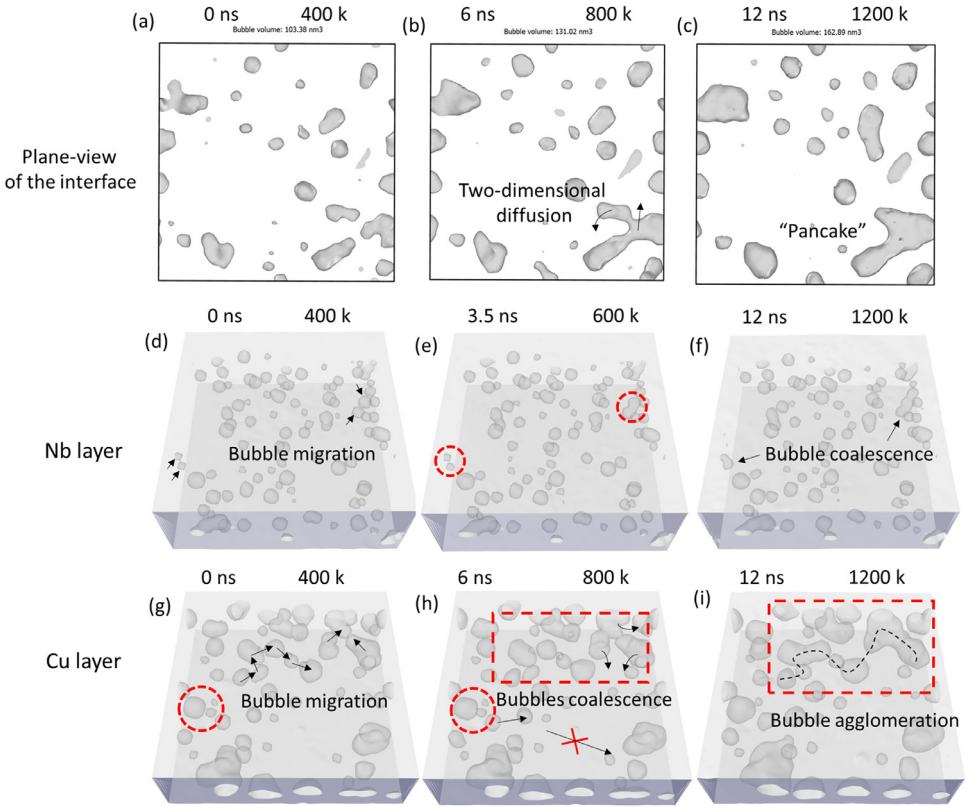

Fig. 3. Diffusive evolution of helium bubble in a Cu/Nb system during the annealing process by MD simulation. (a–c) The plane view of the dynamic evolution of bubbles at the interface. (d–f) A few small bubbles in the Nb layer coalesce via migration within a very short time. (g–i) The construction of bubble agglomerations is more dependent on dense bubbles.

dent surface. It is noted that the location of a micron-sized cavity is deeper than the implanted-helium peak region.

To recap, the formation of outgassing networks seen in our experiments likely depends on both nano-scale diffusive evolution of bubbles activated from lower temperatures and macro-scale displacive fracture at higher temperatures. In principle, the former should be more attractive than the latter for the gentle outgassing purpose. Specifically, as the annealing temperature goes up to around 400°C, small helium bubbles spontaneously coalesce with a "pancake" morphology. As the temperature continues to increase, the size of oblate cavities will grow to a critical flaw size via continuous diffusive processes and volume expansion, triggering the sudden small-scale fracture at as low as 450°C (video S1). The increasing pressure $P_{He}(T(t))$ with rising temperature also provides an additional internal driving force to initiate the cracks. Here, we can estimate the critical flaw size by approximating that all the implanted helium atoms in Cu layers reside in helium cavities like *C* (Fig. 2g) through diffusive processes. Based on the empirical equations-of-state (EOS) expression for high-pressure (on GPa scale) nano helium cavities [14,15] and the critical stress intensity factor [2,16], we calculated the critical flaw size of fracture due to bubble coalescence, as a function of the annealing temperature (Fig. S3). Noted that critical flaw size reduces as rising temperature, in other words, the nanoscaled bubble aggregations are more prone to fracture at higher temperatures (e.g. the size of the cavity C in Fig. 2g and h is much larger than critical fracture size of about 4 nm, see details in Supporting Information).

The displacive fracture facilitates the extension of helium-filled networks, eventually to the free surfaces for helium release. The larger-scale displacive fracture of outgassing networks probably happens after 600°C, after $a(t)$ has grown well beyond nanoscale to tens of microns. As the cavity becomes more oblate, extending along the Cu/Nb interface, the critical stress for crack initiation decreases, causing continuously displacive micro-fracture of oblate cavities nearby (see Fig. S2, with an aspect ratio of cavities > 10), which eventually link up with sample side surfaces (as illustrated in Fig. S2d–f). Moreover, local stress build-up in the helium peak region may initiate microcracks from both above and below the original crack (see insert in Fig. 4g) and the debonding of the layered structure, causing the formation of helium-filled blister cavity (beyond the helium peak region in Fig. 4i). Thus displacive cracks initiating from the weak point of the matrix could connect the cavity to the blistering surface, leading to helium release from the normal surface (as opposed to the side surface), as similarly reported in ref. [17]. Here, taking an example of a blister cavity in Fig. 4i, we measured the diameter of 24 μm and a thickness of 1.2 μm. For average σ_Y of Cu and Nb of 110 MPa, the internal gas pressure at the end of the blister expansion is 22 MPa, according to $P = 2\sigma_Y t / R$ [2], where σ_Y is yield stress, *R*, *t* are radius and thickness of internal cavity, respectively. From van der Waals' equation this pressure corresponds to a helium density of 4.5×10^{20} atoms/cm^3, the total number is 1.2×10^{11} helium atoms in this blister cavity with a volume of 2.72×10^{-10} cm^3 (see Supporting Information for the estimation in this section). The fact that the internal helium pressure P_{He} ~22 MPa at the end-stage is much smaller than its initial ~GPa scale at the diffusive coalescence stage reflects the great displacive expansion in the cavity volume from 450°C to 800°C. Given the helium releasing pattern with strong pulse signals (Fig. 1a) in the high-dose samples, and the sample size, the total implanted helium fluence and the relative release amount measured from the TDS curve, the released helium of 1.1×10^{13} atoms within one pulse (such as peak *D* in Fig. 1a) is estimated to be from around ~100 blisters. Therefore, the massive helium release in a bursting manner above 650°C may be mainly achieved by a large quantity of crack-connected outgassing networks from many blister surfaces simultaneously. On the other hand, the con-

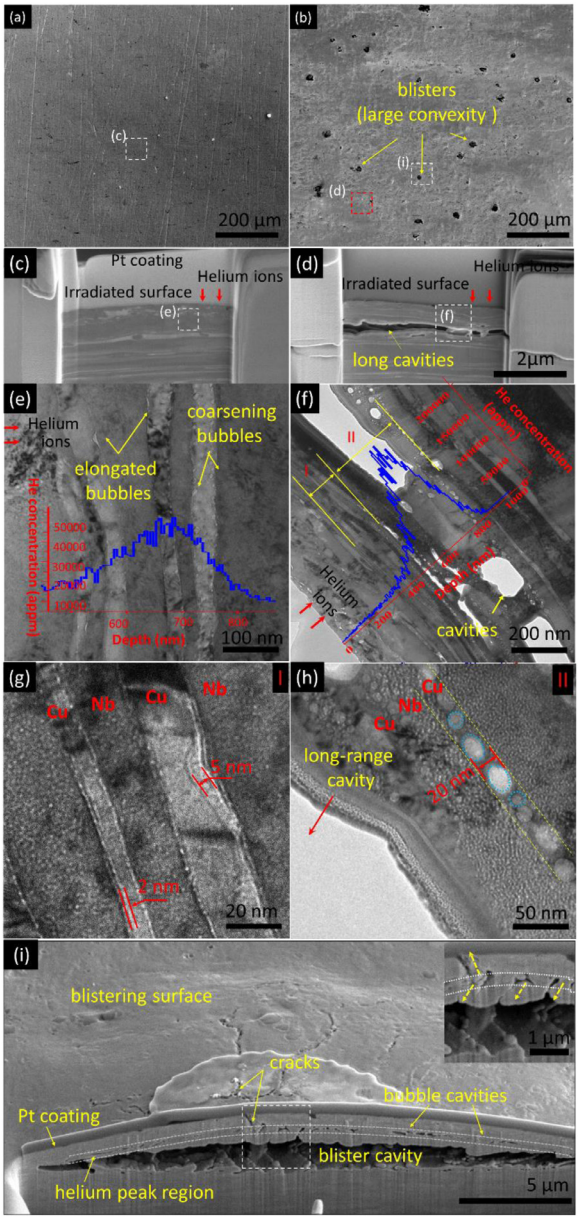

Fig. 4. SEM images of (a) smooth surface and (b) blistering surface of bulk composites with the lowest and the highest doses after the TDS experiments, respectively. (c and d) SEM images of TEM lamellae cut from the smooth region (dashed box in Fig. 4a) and relatively flat blistering region (the red dashed box in Fig. 4b), respectively. (e and f) The magnified cross-sectional TEM images of the dashed boxes in Fig. 4c and d, respectively. SRIM-calculated profiles of helium concentration are also shown as a function of depth for corresponding samples. (g and h) Typical morphology of bubble cavities in areas of I and II in Fig. 4f, respectively. (i) Cracks appear on the lid surface of a large blister. The location of the micron-sized cavity is deeper than the helium peak region, and microcracks initiate from both above and below the original crack. (For interpretation of the references to color in this figure legend, the reader is referred to the web version of this article.).

tinuously gentle gas release (for instance, small peaks like *A* and *B* in Fig. 1a indicate about 10^{10}~10^{11} helium atoms escaping from medium- and high-dose samples) may only require a connection between micron-scaled cavities and the side surfaces. In contrast, for the low dose samples, only elongated bubbles with a small aspect ratio (Fig. 4e) are generated instead of systematic networks connecting to free surfaces; therefore, no macroscopic outgassing was observed even at the high temperature and the irradiated surface is blister-free after the TDS experiment. It still remains to be investigated whether a slower heating rate can lead to an outgassing network without abrupt fracture.

In summary, TDS and in-situ TEM heating experiments and atomistic modeling were carried out to explore the outgassing feasibility in helium irradiated bulk Cu/Nb multilayers. The results show that the massive helium release depends on interconnected outgassing networks constructed through the hybrid diffusive-displacive evolutions of helium bubbles, and the displacive part causes severe degradation of the mechanical integrity. These results suggest that 1D mode of outgassing to avoid structural damage can hardly be achieved in this particular multilayer composite; special 1D structural templating such as heterophase 1D nanowire networks in a single-crystal matrix may be necessary for more stable and effective helium venting in general.

Declaration of Competing Interest

The authors declare that they have no known competing financial interests or personal relationships that could have appeared to influence the work reported in this paper.

Acknowledgment

This work was supported by Eni S.p.A. through the MIT Energy Initiative, and the US DOE Office of Nuclear Energy's NEUP Program under Grant No. DE-NE0008827. We thank Dr. Wayne Kinnison for performing the helium ion irradiation experiments at Texas A&M University. We also thank Dr. Yueqing Yang for assisting the in-situ heating experiment. This research made use of Idaho National Laboratory computing resources which are supported by the Office of Nuclear Energy of the U.S. Department of Energy and the Nuclear Science User Facilities under Contract No. DE-AC07-05ID14517. Also, R.G., L-F.Z., X-P.W. and Q-F.F. acknowledge support by the National Natural Science Foundation of China (Grant Nos. 12005256, U1967211, 51771181, 51801194, 51971212), and the Anhui Provincial Natural Science Foundation (Grant No. 1908085QA42) .

Supplementary materials

Supplementary material associated with this article can be found, in the online version, at doi:10.1016/j.scriptamat.2020.113706.

References

[1] M.R. Gilbert, S.L. Dudarev, S. Zheng, L.W. Packer, J.C. Sublet, Nucl. Fusion 52 (8) (2012) 083019.
[2] J.H. Evans, J. Nucl. Mater. 68 (1977) 129–140.
[3] K.P. So, D. Chen, A. Kushima, M. Li, S. Kim, Y. Yang, Z. Wang, J.G. Park, Y.H. Lee, R.I. Gonzalez, M. Kiwi, E.M. Bringa, L. Shao, J. Li, Nano Energy 22 (2016) 319–327.
[4] D. Chen, N. Li, D. Yuryev, J.K. Baldwin, Y. Wang, M.J. Demkowicz, Sci. Adv. 3 (2017) eaao2710.
[5] M.J. Demkowicz, Y.Q. Wang, R.G. Hoagland, O. Anderoglu, Nucl. Instrum. Methods Phys. Res. Sect. B 261 (1-2) (2007) 524–528.
[6] R. Gao, M. Jin, F. Han, B. Wang, X. Wang, Q. Fang, Y. Dong, C. Sun, L. Shao, M. Li, J. Li, Acta Mater. 197 (2020) 212–223.
[7] L.F Zhang, R. Gao, B.L Zhao, M. Sun, K. Jing, X.P. Wang, T. Hao, Z.M. Xie, Q.F. Fang, C.S. Liu, J. Alloys Compd. 827 (2020) 154312.
[8] R.E. Stoller, M.B. Toloczko, G.S. Was, A.G. Certain, S. Dwaraknath, F.A. Garner, Nucl. Instrum. Methods Phys. Res. Sect. B 310 (2013) 75–80.
[9] S. Plimpton, J. Comput. Phys. 117 (1995) 1–19.
[10] A. Kashinath, M.J. Demkowicz, Model. Simul. Mater. Sci. Eng. 19 (3) (2011) 035007.
[11] E. Kautto, J. Kuhalainen, M. Manninen, J. Phys. 9 (1997) 4365–4376.
[12] J.A.F. Plateau, G.-V. Paris (1873).
[13] B.K. Derby, J.K. Baldwin, D. Chen, M.J. Demkowicz, Y.Q. Wang, A. Misra, N. Li, JOM 72 (1) (2020) 145–149.
[14] N. Li, M. Nastasi, A. Misra, Int. J. Plast. 32-33 (2012) 1–16.
[15] R.L. Mills, D.H. Liebenberg, J.C. Bronson, Phys. Rev. B 21 (11) (1980) 5137–5148.
[16] J.H. Evans, A. Van Veen, J.TH.M. De Hosson, R. Bullough, J.R. Wills, J. Nucl. Mater. 125 (1984) 298–303.
[17] W.M. Shu, E. Wakai, T. Yamanishi, Nucl. Fusion 47 (3) (2007) 201–209.

Supporting Information

Hybrid diffusive-displacive helium outgassing in Cu/Nb multilayer composites

Rui Gao, Miaomiao Jin, Qingjie Li, Kang Pyo So, Lifeng Zhang, Xianping Wang, Qianfeng Fang, Cheng Sun, Lin Shao, Ju Li

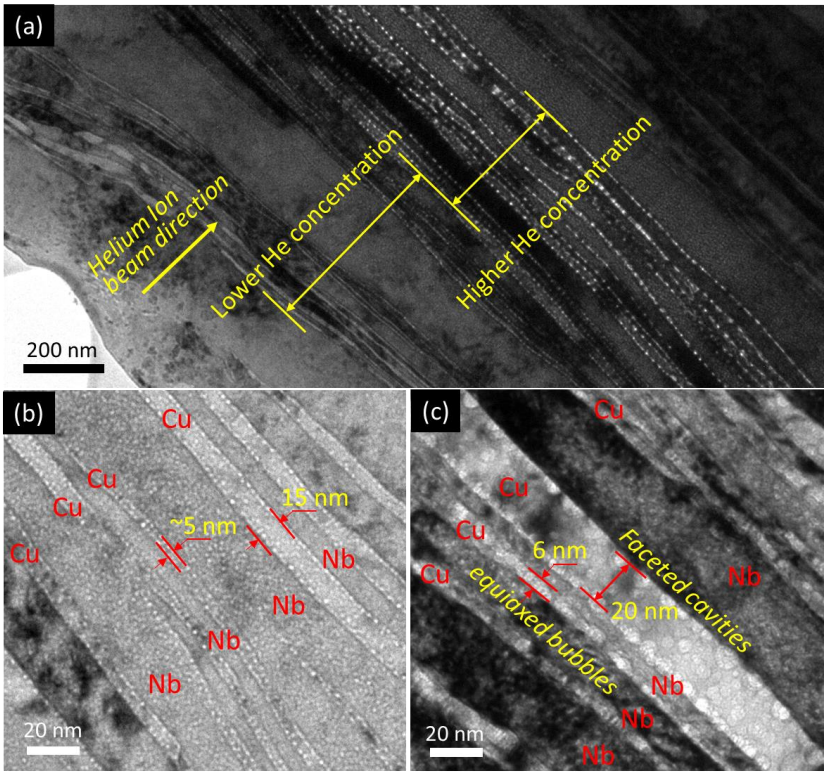

Fig. S1. (a) The cross-sectional TEM image shows the bubble distribution across the helium implanted region of a Cu/Nb multilayer with a fluence of 5×10^{17} ions/cm^2. Different bubble morphologies in the region with (b) a lower helium concentration and (c) a higher helium concentration.

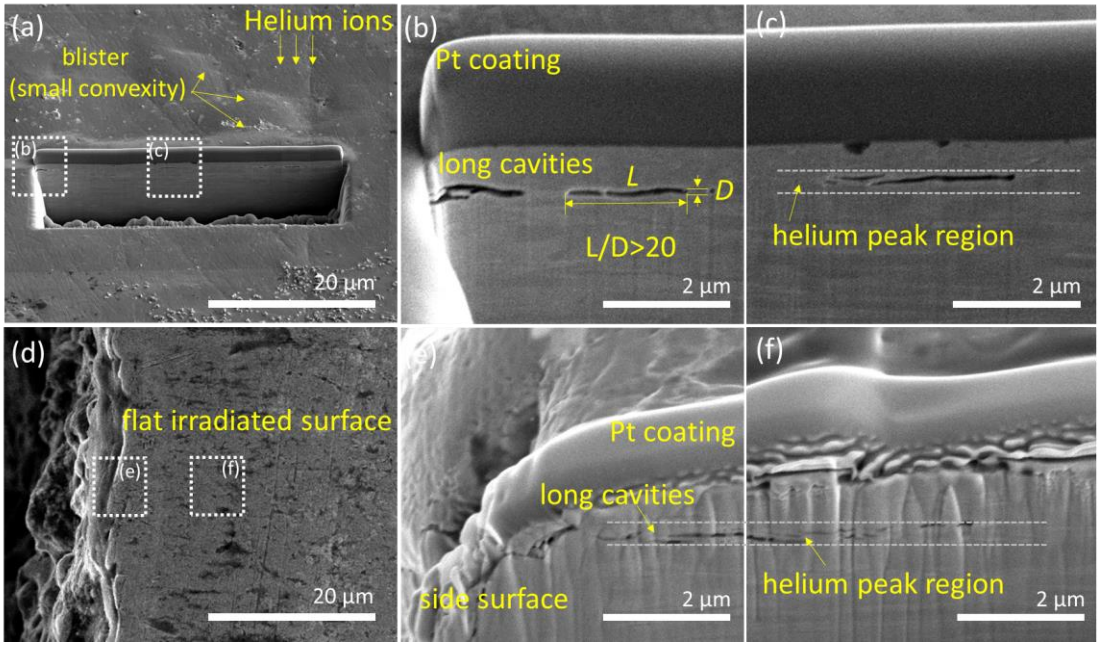

Fig. S2. (a,b,c) SEM images of the relatively flat (small convexity) blistering surfaces illustrate long cavities with a large aspect ratio located in the helium peak region from a cross-sectional view. (d) SEM image of relatively flat irradiated surface close to the sample side surface. (e, f) Long cavities filled with helium can connect to the sample side surface from a cross-sectional view.

The critical crack length of bubble agglomeration fracture as a function of the annealing temperature.

In the following estimation, we just consider bubble behaviors in the helium peak region of Cu layers in the highest-dose sample. The molar volume of helium in those bubble agglomerations can be described by the empirical equations-of-state (EOS) expression for high-pressure helium bubbles [1, 2]:

$$V_{molar\,He} = (22.575 + 0.006455\,T - 7.2645\,T^{-1/2})\,P^{-1/3} + (-12.483 - 0.024549T)P^{-2/3} + (1.0596 + 0.10604T - 19.641T^{-1/2} + 189.84T^{-1})P^{-1} \quad (1)$$

where P is the pressure (kbar) and T is the absolute temperature.

$$V_{molar\,He} = \frac{N_{bubbles}\,V_{bubble}\,N_0}{N_{He}} \quad (2)$$

where $N_{bubbles}$ is the number of bubble agglomerations (taking an example with the size of 25 nm × 25 nm × 5 nm) with "pancake" morphology in a given area, which is measured by TEM images; V_{bubble} is the average volume of the bubble agglomerations, N_0 is Avogadro's constant, N_{He} is the total number of helium atoms in those bubble agglomerations estimated through the helium dose (5×10^{17} ions/cm^2) and SRIM calculation (about 21% of total implanted helium atoms in helium peak region of Cu layers). Here, the $V_{molar\,He}$ of around 5.4 cm^3/mol was calculated according to Eq. (1) and (2). Following the theory by Evans et al. [3, 4], to obtain the critical crack length a_c, for the gas-filled cracks, we note the critical stress intensity factor K_{IC} and internal pressure P,

$$K_{IC} = P\left[\frac{\pi a_c}{2}\right]^{1/2} + \frac{\mu b}{(1-\nu)(2\pi a_c)^{1/2}} \quad (3)$$

$$P = \frac{\mu b}{(1-\nu)\pi a_0}\left[\left[\frac{a_0}{a_c}\right]^{1/2} - \frac{a_0}{a_c}\right] \quad (4)$$

where μ is the shear modulus of Cu matrix (48 GPa), b is the Burgers vector (0.256 nm), and ν is Poisson's ratio (0.34), a_0 (0.09 nm) is defined as the corresponding equilibrium length of the crack containing no gas [4]. Combining Eq. (1)-(4), we got the critical crack length a_c of bubble agglomeration fracture as a function of the annealing temperature and their internal pressure.

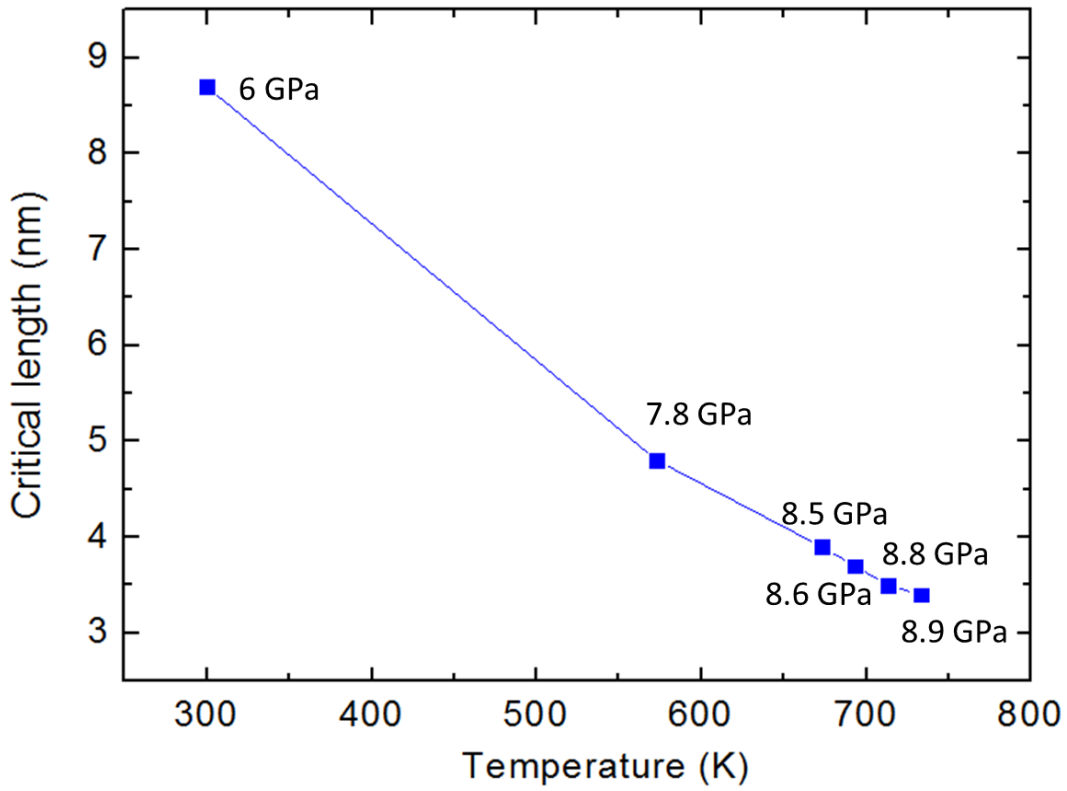

Fig. S3. The critical crack length of bubble agglomeration fracture as a function of the annealing temperature and their internal pressure.

The estimation of released helium atoms within one pulse in the TDS curve of the highest-dose sample.

The total helium fluence in the highest-dose bulk sample is 1.25×10^{17} ions based on the irradiated surface area of 0.25 cm^2. According to the TDS curve, we approximate that the amount of released helium with increasing temperature follows the normal distribution, therefore, about 90% of implanted helium in Cu layers is estimated to be discharged when the sample is annealed at 800°C depending on the extrapolated fitting curve (Fig. S4). The number of escaped helium atoms represented by peaks *A*, *B*, *C*, *D* in the TDS curve is estimated to be 3×10^{10}, 4.5×10^{11}, 6×10^{12}, 1.1×10^{13} atoms, respectively, according to the ratio of four peaks values (i.e. 50, 680, 9000, 17000, respectively) to the total value of mass response signal.

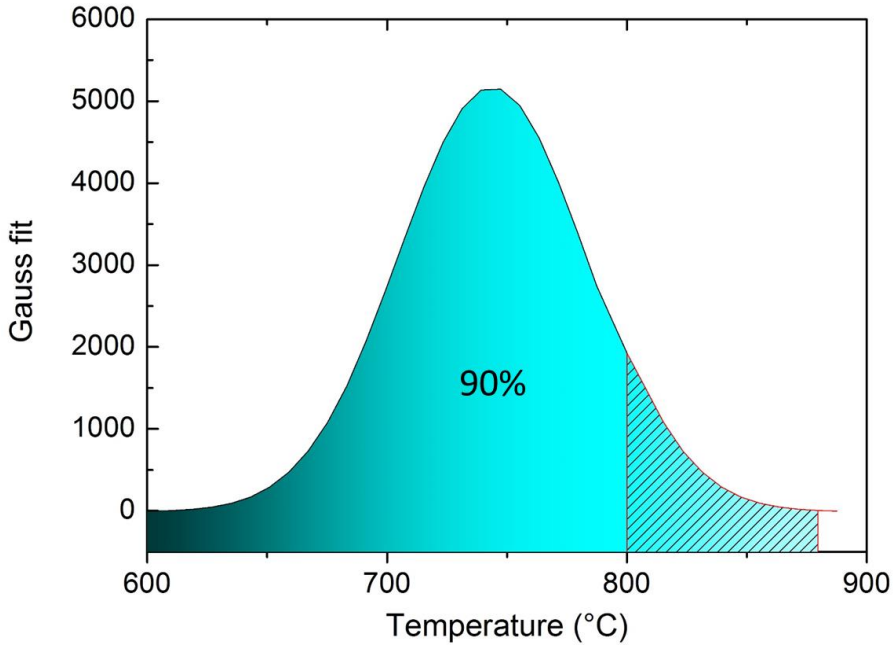

Fig. S4. About 90% of implanted helium in Cu layers is estimated to be discharged when the sample is annealed at 800°C depending on the extrapolated fitting curve.

The estimation of released helium atoms within one blister cavity.

Taking an example of a blister in Fig. 4i, if the blister cavity deformation is approximated to that of a thin spherical shell (see Fig. S5) under the internal pressure, P, the deformation will stop when the internal shell radius, R, reaches a value given by $P = 2\sigma_Y t / R$ [3], where t is the shell (blister cavity) thickness and σ_Y is yield stress. Here, for average σ_Y of Cu and Nb of 110 MN/m^2, the cavity radius R of 12 μm and thickness t of 1.2 μm, the internal gas pressure at the end of the blister expansion is 22 MPa. From Van der Waals' equation $P(v-b)=RT$ [5] (with b = 23.8 cm^3/mol), where v is the volume of the container occupied by each particle, R is the universal gas constant, T is temperature, this pressure corresponds to a helium density of 4.5×10^{20} atoms/cm^3, and the total number is 1.2×10^{11} helium atoms in this blister cavity with a volume of 2.72×10^{-10} cm^3.

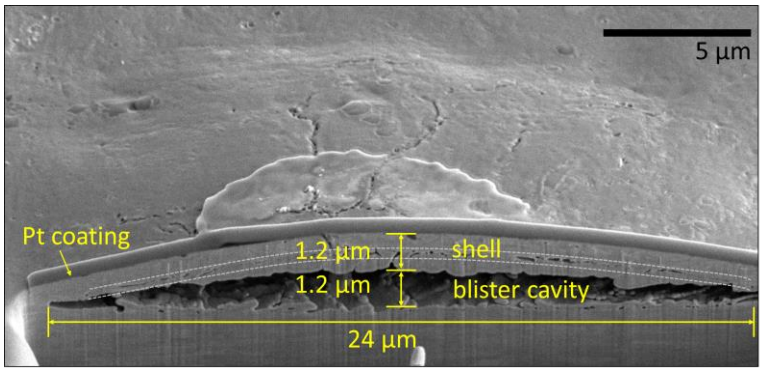

Fig. S5. The size parameters of the blister cavity in Fig. 4i.

References:

[1] N. Li, M. Nastasi, A. Misra. Defect structures and hardening mechanisms in high dose helium ion implanted Cu and Cu/Nb multilayer thin films, International Journal of Plasticity 32-33 (2012) 1-16.

[2] R.L. Mills, D.H. Liebenberg, J.C. Bronson. Equation of state and melting properties ofHe^4 from measurements to 20 kbar, Physical Review B 21 (1980) 5137-5148.

[3] J.H. Evans. An interbubble fracture mechanism of blister formation on helium-irradiated metals, Journal of Nuclear Materials 68 (1977) 129-140.

[4] J.H. Evans, A. Van Veen, J.TH.M. De Hosson, R. Bullough and J.R. Wills. THE TRAPPING OF HELIUM AT A LOW ANGLE TILT BOUNDARY IN MOLYBDENUM, Journal of Nuclear Materials 125 (1984) 298-303.

[5] J.W. Harrison. AN EXTRAPOLATED EQUATrON OF STATE FOR XENON FOR USE IN FUEL SWELLING CALCULATIONS, Journal of Nuclear Materials 31 (1969) 99-106.